



ARTICLE

Bond Behavior between BFRP Bars and Hybrid Fiber Recycled Aggregate Concrete after High Temperature

Boheng Zhu¹, Huaxin Liu^{1,*}, Genjin Liu², Abasal Hussain², Xiaofei Zhang³ and Xuezhi Wang¹

¹College of Civil and Architectural Engineering, Liaoning University of Technology, Jinzhou, 121000, China

²State Key Laboratory of Coastal and Offshore Engineering, Dalian University of Technology, Dalian, 116024, China

³Institute of Water Resources and Hydro-electric Engineering, Xi'an University of Technology, Xi'an, 710048, China

*Corresponding Author: Huaxin Liu. Email: lgliuhuaxin@163.com

Received: 11 August 2020 Accepted: 30 September 2020

ABSTRACT

The aim of this study is to improve the bond performance of basalt fiber reinforced polymer (BFRP) bars and recycled aggregate concrete (RAC) after being exposed to high temperatures. The bond behavior (failure modes, bond strength, bond stress-slip curves) between BFRP bars and hybrid fiber recycled aggregate concrete (HFRAC) after being exposed to temperatures ranging from 20°C up to 500°C was studied by using pull-out tests. The effect of high temperatures on mechanical properties of concrete (compressive strength, splitting tensile strength) and tensile strength of BFRP bars was also investigated. The bond strength decreased as the temperature increased and the drop of bond strength between RAC and BFRP bar was larger than that between HFRAC and BFRP bar. As the temperature rises, the key factor affecting the bond strength was gradually transformed from concrete strength to BFRP bar strength. The relationship between bond stress and slip in the dimensionless bond stress-slip ascending section was established, which was in good agreement with the experimental results.

KEYWORDS

High temperature; BFRP bar; hybrid fiber; recycled aggregate concrete; bond performance

1 Introduction

As a new type of concrete material from waste buildings, the recycled aggregate can be used to partially or entirely replace natural aggregates to prepare recycled aggregate concrete (RAC), which has good social and economic benefits [1,2]. Compared with natural aggregate concrete (NAC), RAC has more pores and interface transition zones (ITZs), which results in lower mechanical properties [3–7]. Previous studies have shown that a suitable amount of fiber can effectively restrain the development of internal cracks in concrete and reduce stress concentration at cracks, thus improve mechanical properties such as tensile, flexural, impact and fire resistance of concrete. Especially when two or more fibers of different properties are mixed into concrete, they exert their advantages in different aspects and loading stages and show a positive synergistic effect, resulting in higher toughness and cracking resistance ability [8–11]. After mixing polypropylene fiber and steel fiber, the RAC tensile strength and bending strength improved significantly [8]. The synergy of macro-steel fiber and micro-cellulose fiber was studied through bending



tests in literature [9]; the results showed that the toughness of concrete could hardly be improved by the single use of cellulose fiber, but it shows a significant positive effect on improving the toughness of concrete in the presence of steel fibers. The hybrid use of steel and polypropylene fibers can effectively improve the fire resistance of concrete at high temperature [10]. A previous study also demonstrated that there was a positive effect on the dynamic performance by adding the glass fiber and polypropylene fiber into concrete [11].

Fiber reinforced polymer bars (FRP bars) show excellent corrosion resistance, fatigue resistance, lightweight, high strength and non-electromagnetic properties [12–14], and have broad application prospects. Similar to conventional reinforced concrete structures, the bond between FRP bars and concrete is the basis of their joint work. The bond strength between BFRP bars and concrete after freeze-thaw cycles was studied through pull-out tests, and the results showed that 200 freeze-thaw cycles have little effect on the bond strength of BFRP bars [15]. The bond durability of FRP bars under seawater conditions was investigated in literature [16], and the results showed that surface sand-coating reduced the short-term bond strength but significantly improved the bond durability for the ribbed BFRP bars. The bond durability of different FRP bars and concrete in alkaline environment was studied in the literature [17], and the results showed that the order of bond durability strength was CFRP (carbon fiber reinforced polymer) bar > BFRP bar > GFRP (glass fiber reinforced polymer) bar. The bond strength of GFRP bars under fatigue loads was studied through pull-out tests, and the results showed that the bond strength of GFRP bar was reduced by 63%–70% compared with the static bond strength after 2 million cyclic loads [18]. The investigation for bond strength of FRP-concrete subjected to fatigue loads in the hygrothermal environment showed that the bond behavior of the FRP-concrete interface was reduced in the hygrothermal environment. In addition, the fatigue life of the specimens pretreated with wet-heat was significantly shorter than that of the untreated specimens [19]. Existing experimental research results showed that high temperature has a significant negative effect on the mechanical properties of FRP bars [20–22]. Previous studies concentrated on the bond behavior of FRP and concrete subjected to high temperature and the highest temperature was no more than 350°C [23,24]; however, there was less research on the residual bond behavior between FRP bars and concrete after high temperature exposure.

In this work, the bond behavior (failure modes, bond strength, bond stress-slip curves) between BFRP bars and hybrid fiber reinforced recycled aggregate concrete (HFRAC) after high temperature exposure was investigated. The research results can be used as an experimental and theoretical reference for fire prevention design and fire safety evaluation of FRP bar reinforced fiber recycled concrete.

2 Test Overview

2.1 Materials and Experimental Parameters

The diameter of the BFRP bars was 12 mm, the surface of which was extruded into ribs and bonded with sand. The measured tensile strength and elastic modulus of the BFRP bars were 1114 MPa and 47.5 GPa, respectively. By referring to previous literature [25,26], the temperature of the tests included 20°C, 100°C, 200°C, 300°C, 400°C and 500°C. The recycled coarse aggregate was taken from an abandoned building, and the strength of the original concrete was about 30 MPa. The properties of coarse aggregate are shown in Tab. 1. The schematic diagram of the test specimen is shown in Fig. 1. The concrete mix was made of ordinary Portland cement grade 42.5; the natural river sand and tap water were used; the replacement rate of recycled coarse aggregate was 50% in 5–20 mm continuous grading coarse aggregate, which was soaked for 12 h before the test to compensate its water absorption; the fiber types and performance index are shown in Tab. 2. The volume content of basalt fiber was 0.15% of the concrete volume, so was the cellulose fiber. Concrete was cast with the following mix design per m³: 476 kg cement, 713 kg sand, 490 kg recycled coarse aggregate, 490 kg natural coarse aggregate, and 225 kg water. For pull-out specimens, the BFRP bars were cut into 500 mm lengths, and the encasing concrete

cube had dimensions of $150 \times 150 \times 150$ mm. The BFRP bars were concentrically embedded in the concrete with bond lengths of $5d$ (d is the diameter of bar 12 mm). The BFRP bars were prepared with ceramic sleeves to control the bond lengths. Both ends of the ceramic sleeve were sealed with a small amount of paraffin, which played the role of preventing mortar pouring. The end of BFRP bars was anchored by a steel pipe with expansive cement to avoid the shear damage of BFRP bars by clamps. To facilitate the analysis of the results, concrete cubic compressive strength tests, cubic splitting tensile strength tests and BFRP bar tensile strength tests exposed to different temperatures were also carried out. For BFRP bar tensile strength tests, the BFRP bars were cut into 520 mm lengths. The above parameters were referenced from previous studies [27–29].

Table 1: The properties of coarse aggregate

Type of coarse aggregate	Particle size/mm	Apparent density/kg·m ⁻³	Bulk density/kg·m ⁻³	Water absorption/%	Crushing index/%
Natural coarse aggregate	5~20	2830	1485	0.56	13.71
Recycled coarse aggregate	5~20	2530	1296	8.33	8.93

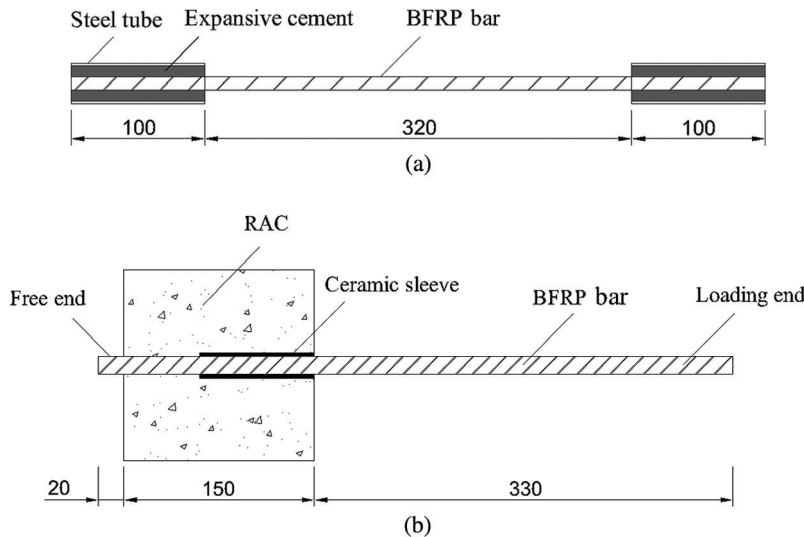


Figure 1: Diagram of the specimens (unit: mm) (a) BFRP tensile specimen, (b) Pull-out specimen

Table 2: Fiber characteristics (according to manufacturer's data)

Type of fiber	Diameter/ μm	Length/mm	Density/g·cm ⁻³	Tensile strength/MPa	Elastic modulus/GPa	Denier/g·9000 m ⁻¹	Elongation at break/%
Basalt fiber	16	12	2.65~3.05	3000~3500	90~110	–	3.2
Cellulose fiber	17.9	2.1	1.11	913	9.25	2.5	–

2.2 Specimens Production

The cement, sand, natural coarse aggregate and recycled coarse aggregate were dry mixed in the first. Then, half of the water was gradually added to the dry mix in the running spiral stirrer. Finally, in an attempt of assuring a suitable distribution of hybrid fibers, the blended BF, CF and remaining water were gradually added to the mixture. The specimens were demoulded after 24 hours and transferred to curing room for 28 days. The curing room was set at $20 \pm 2^\circ\text{C}$ with approximately 95% humidity. After three months, the

specimens were tested by pull-out tests. The most common test procedures used to evaluate the bond behavior are the pull-out test, the splice test and the beam test. The specimens of the beam test and splice test are large in size and complex in fabrication. Compared with other test methods, the pull-out test was more straightforward and more suitable for comparing the relative bond properties [30]. To ensure the reliability of the test results, five specimens were made for each group of pull-out specimens. The specimens to be tested are shown in Fig. 2.



Figure 2: The specimens for pull-out tests in laboratory

2.3 Test Device and Loading Equipment

The high-temperature furnace used in the test was equipped with a temperature control system and the heating rate was 10°C/min. The specimens were placed in batches and kept at a constant temperature for 5 h [31], after which they were naturally cooled to room temperature. To prevent the exposed BFRP bar on the outside of the pull-out specimen from being damaged by high temperature and affecting the test results, the surface was treated with fire-resistant paint and fireproof asbestos before testing. In the pre-test, the K-type thermocouple was used to measure the temperature-time curves of the concrete cubes at different temperatures, as shown in Fig. 3. The pull-out test was controlled by displacement, and the deformation rate was 0.2 mm/min. The free end slip of BFRP bars was measured by a linear variable differential transformer (LVDT). During the test, the load and displacement of the free end slip of the BFRP bar were recorded by the data acquisition system in real time. The self-made reaction force cage device avoided the tearing of the concrete caused by the eccentricity of the BFRP bar by adjusting the bolt, as shown in Fig. 4.

3 Strength of Concrete and BFRP Bar after High Temperature

The tests of the material properties of BFRP bars and concrete after different temperatures were carried out to facilitate the analysis of the results of pull-out tests. The concrete cubic compressive strength and splitting tensile strength tests were conducted according to GB/T 50081-2019 standard [32], using a 5000 kN universal testing machine. The tensile strength tests of BFRP bars were carried out according to GB/T 50152-2012 standard [29], using a 300 kN universal testing machine.

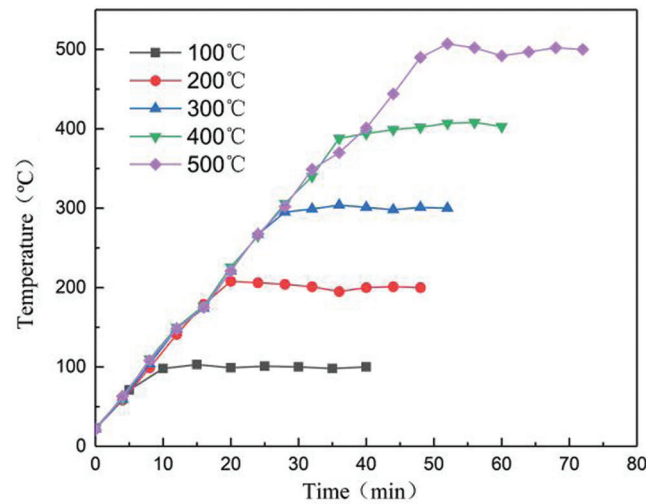


Figure 3: Temperature-time curves of concrete cubes at different target temperatures

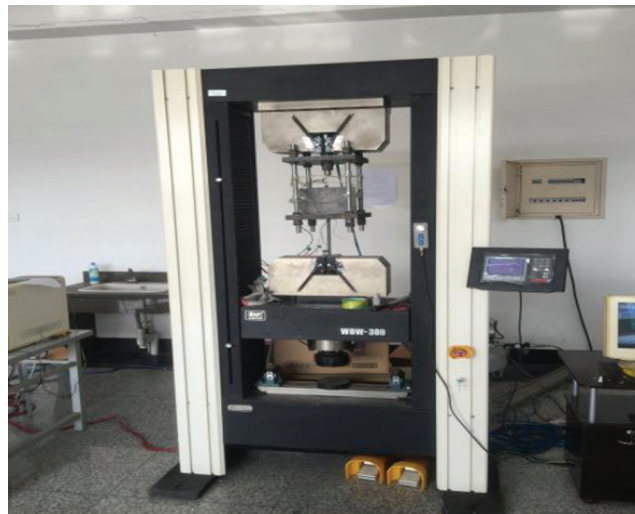


Figure 4: The pull-out test setup

3.1 Concrete Strength after Different Temperatures

The concrete cubic compressive strength and splitting tensile strength of HFRAC and RAC (control group) after different temperatures are shown in Figs. 5 and 6, respectively. Obviously, the concrete strength of HFRAC specimens was better than those of RAC. It was attributed to the restraint effect of hybrid fibers on the deterioration of pore structure of the concrete matrix at high temperature [33], thus improved the RAC splitting tensile performance after high temperature exposure. As the temperature increased, the concrete cubic compressive strength of HFRAC increased first and then decreased, reaching a peak at 400°C. Except for “high temperature curing” at 400°C, the overall properties of RAC showed a downward trend. When the temperature raised from 300°C to 400°C, the RAC strength was increased. The RAC is equivalent to undergoing a high temperature curing process, which makes the cement hydration reaction more fully [34]. However, obvious strength loss was observed for the RAC after expose to more than 400°C temperature.

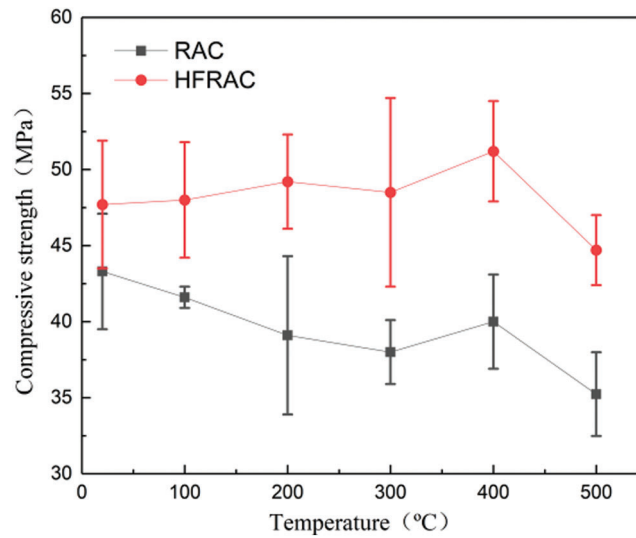


Figure 5: Compressive strength of concrete

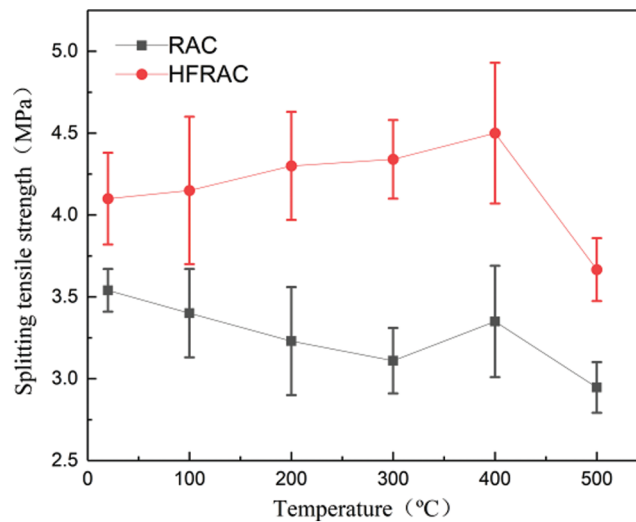


Figure 6: Splitting tensile strength of concrete

3.2 Mechanical Properties of BFRP Bars after Different Temperatures

See Tab. 3 and Fig. 7 for the tensile strength and relative tensile strength of BFRP bars after target temperatures. Before 300°C, the tensile strength of BFRP bars decreased slowly with the increase of temperature by about 12%. After 300°C, the tensile strength of BFRP bars decreased sharply, and the strength at 400°C was only 11%. Based on the test results, the sudden drop in the tensile strength occurred between 300°C and 400°C, was due to the thermal degradation of the epoxy resin, as pointed out in literature [35]. Below 300°C, the properties of BFRP bars can be recovered when the specimens were heated and then tested at room temperature. However, after prolonged exposure to high temperature (above 300°C) and an oxygen-deficient environment, the resin was carbonized and decomposed from the outside to the inside, thereby losing its binding effect to the fiber bundle [23,36]. In addition, high temperature also caused unfavorable damage to the fiber, which significantly reduced the cooperative working ability of the fiber bundle and epoxy resin. After 500°C, the epoxy resin matrix on the surface of

the BFRP bars was completely ignited and decomposed, exposing the softened fiber bundles, and the tensile test was no longer possible, as shown in Fig. 8.

Table 3: Tensile strength of BFRP bars after target temperatures

$T/^\circ\text{C}$	20	100	200	300	400	500
Tensile strength/MPa	1114	1064	1019	979.2	118.2	–

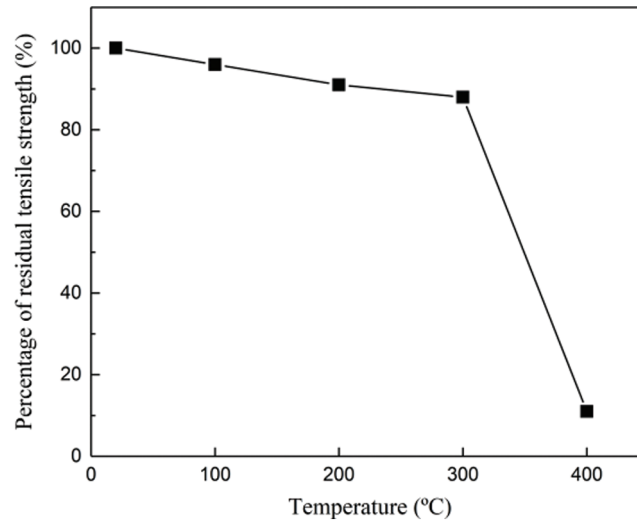


Figure 7: The ratio of tensile strength of BFRP bars before and after being exposed to high temperatures



Figure 8: BFRP bar after 500°C

4 Pull-Out Test Results and Discussion

In this experiment, the pull-out tests were carried out to evaluate the bond properties of BFRP bars and HFRAC. The following Eq. (1) was used to calculate the value of bond strength. The main results of

the pull-out test are shown in Tab. 4. The specimen ID meaning: concrete type + test temperature, such as HH100 means HFRAC after being exposed to 100°C, HN200 means RAC after being exposed to 200°C.

$$\tau = \frac{p}{\pi dL} \quad (1)$$

Note: τ is the bond strength (MPa); p is the maximum tensile force (N); d is the diameter of BFRP bar (mm); L is the bonded length (mm).

Table 4: The results of pull-out tests

$T/^\circ\text{C}$	Specimen ID	τ_u/MPa	s_u/mm	Failure mode
20	HN20	17.92 ± 0.96	2.61 ± 0.21	P
	HH20	18.96 ± 0.99	3.24 ± 0.11	P
100	HN100	16.25 ± 1.05	3.11 ± 0.20	P
	HH100	19.57 ± 1.13	5.02 ± 0.16	P
200	HN200	14.08 ± 0.87	5.47 ± 0.25	P(with cracks)
	HH200	20.15 ± 1.13	7.33 ± 0.17	P
300	HN300	9.78 ± 0.65	7.06 ± 0.29	P(with cracks)
	HH300	15.51 ± 0.51	7.92 ± 0.46	P
400	HN400	5.53 ± 0.24	7.32 ± 0.17	P
	HH400	6.23 ± 0.29	7.32 ± 0.22	P
500	HN500	–	–	FRP bar fracture
	HH500	–	–	FRP bar fracture

Note: Data are presented as means \pm standard deviations; τ_u is the peak bond strength; s_u is the slip corresponding to the peak bond strength; P is pull-out failure.

4.1 Failure Modes

Most specimens failed by pull-out failure of the BFRP bar, of which HN200 and HN300 specimens failed with concrete cracks, as shown in Fig. 9. This indicated that after being exposed to 200°C and 300°C, the tensile strength of RAC was slightly lower than the radial component force of BFRP bars under loading, so pull-out failure with cracks occurred. When HN500 and HH500 were tested, the BFRP bars were fractured before the sliding of the free end, and no data were collected.

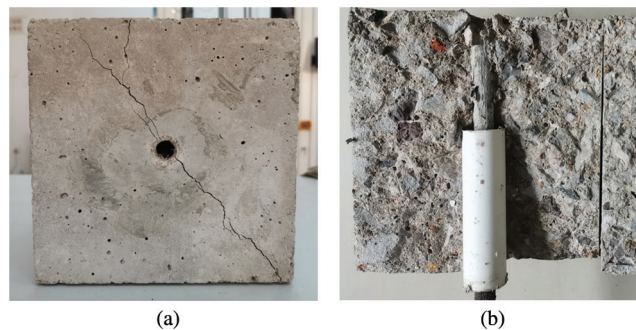


Figure 9: Pull-out failure specimen with cracks (a) front, (b) section profile

4.2 Bond Stress-Slip Curves

The bond stress-slip curves of the pull-out specimens after being exposed to different temperatures are summarized in Fig. 10, where Fig. 10(a) represents the RAC specimen and Fig. 10(b) represents the HFRAC specimen. The slope of each curve decreased gradually with the increase of temperature, which indicated the bond elastic modulus decreased with the increasing exposure temperature. Obviously, the peak bond strength of RAC specimens decreased as the temperature increased. Before 200°C, the peak bond strength of RAC specimens slightly decreased by about 21%, and the drop accelerated after 300°C. At 400°C, the peak bond strength of RAC specimens was only 31%. In addition, as the temperature increased, the peak slip value gradually increased. For HFRAC, as the temperature increased, the peak bond strength increased first and then decreased. Before 200°C, the peak bond strength of the HFRAC specimens increased slightly, about 12%, and then dropped rapidly after 200°C. At 400°C, the peak bond strength of HFRAC specimens was only 35%. The changing trend of the peak bond strength of RAC and HFRAC specimens before 300°C was similar to that of the corresponding concrete cubic compressive strength and splitting tensile strength, so the main factor determining the bond strength at this stage was the mechanical properties of concrete. There was a reason that caused the above results. BFRP bars had a higher transverse coefficient of thermal expansion (CTE) than that of concrete. When the temperature rose, tensile stress was generated in concrete, which produced cracks and reduced bond strength. The molten cavity formed after cellulose fiber (CF) melting in HFRAC helped to balance the temperature of the matrix and reduced the internal stress caused by the temperature gradient. In addition, basalt fiber (BF) was tightly bonded with the concrete matrix to form space integrity, which increased the bond strength. After 300°C treatment and cooling down to room temperature, the tensile strength of BFRP bars recovered to 92%, which could be considered has a little negative effect on the bond strength. However, the bond strength of each group of RAC specimens was greatly reduced after 300°C, which was significantly different from the corresponding cubic compression and splitting tensile strength. The tensile strength of BFRP bars at 300°C and 400°C was 83% and 11% of that at room temperature, respectively. There was a reason that caused the above result. Above 300°C, the epoxy resin inside the BFRP bar began to carbonize under an anoxic state. Even if the tensile tests of FRP bars were performed after the bar cooling, experimental studies showed that irreversible loss of mechanical properties occurs for temperature above 300°C, and no strength recovery can take place [35]. Consequently, above 300°C, the key factor controlling the bond strength was no longer the mechanical properties of concrete, but the strength of the BFRP bars. The bond strength of HFRAC was higher than that of RAC at all target temperatures. The peak bond strength of HFRAC after 20°C, 100°C, 200°C and 300°C was 6%, 20%, 36% and 58% higher than that of RAC, respectively, indicating the incorporation of CF and BF reduced the damage of high temperature to RAC and significantly improved the bond performance of BFRP bar and RAC.

Besides, the formulas showing the relation between the peak bond strength of RAC and HFRAC with respect to temperature were established through the test data, as shown in Eqs. (2) and (3), respectively, and the fitting curves were shown in Fig. 11.

$$\tau_u = 18.15 - 1.24(T/100) - 0.48(T/100)^2 \quad R^2 = 0.957 \quad (2)$$

$$\tau_u = 17.52 + 5.03(T/100) - 1.94(T/100)^2 \quad R^2 = 0.937 \quad (3)$$

Take the ascending segments of the bond stress-slip curves to draw dimensionless bond stress-slip curves, as shown in Fig. 12, where Fig. 12(a) represents RAC and Fig. 12(b) represents HFRAC. The trends of HN20 and HN100 curves were similar, showing a convex trend, which indicated that the bond stress-slip relationship between BFRP bars and RAC changed little after being exposed to 100°C. The curves of HN200, HN300 and HN400 showed a similar concave trend, but were quite different from the

curves of HN20 and HN100, which indicated that the bond stress-slip relationship changed significantly after temperature higher than 200°C. The trends of HH20, HH100, HH200, and HH300 curves were similar, showing a convex trend, which indicated that the bond stress-slip relationship between BFRP bars and HFRAC exhibited little change after being exposed to a temperature not higher than 300°C. The curve of HH400 showed a concave trend, indicating that the bond stress-slip relationship between BFRP bars and HFRAC changed obviously after 400°C treatment. Therefore, it can be concluded that high temperature is the key factor in changing the trend of dimensionless bond stress-slip curves of RAC and HFRAC. The incorporation of hybrid fibers improved the bond performance of RAC after high temperature exposure, thereby delaying the change of bond stress-slip relationship caused by high temperature exposure. For both RAC and HFRAC, it is necessary to propose two kinds of bond stress-slip relationships for convex and concave curve trends.

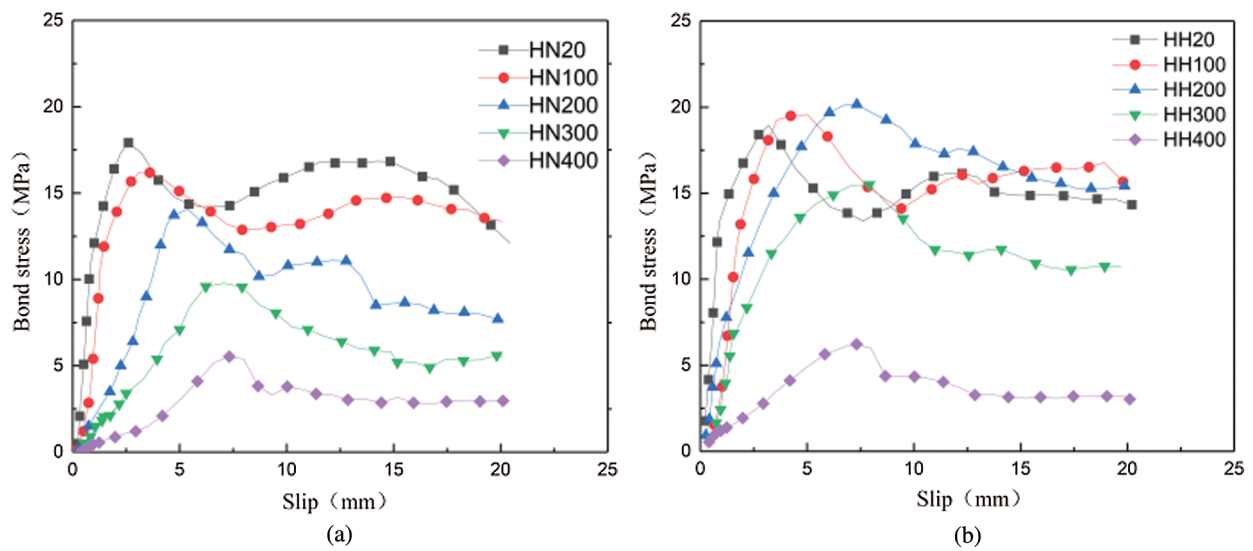


Figure 10: The bond-slip curves at different temperatures (a) RAC, (b) HFRAC

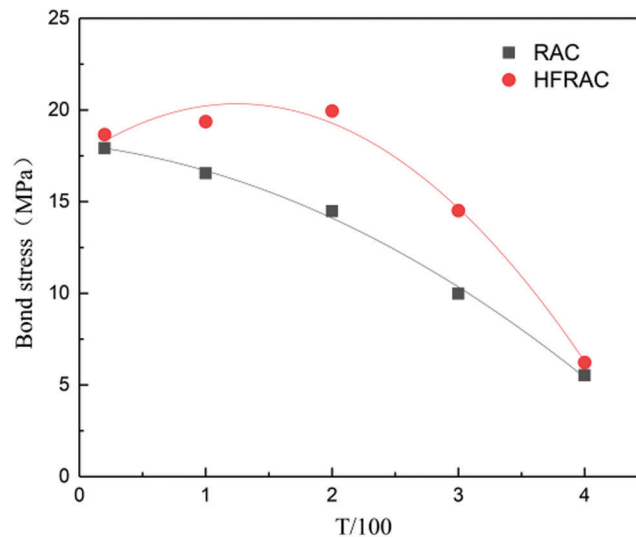


Figure 11: Fitting curves between peak bond strength and temperature

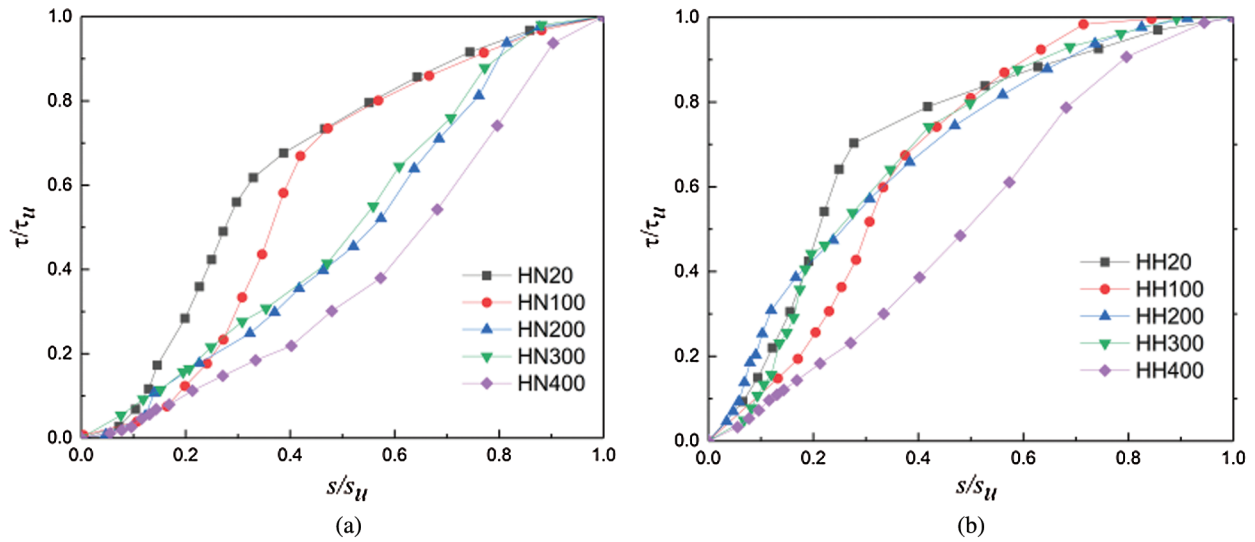


Figure 12: Non-dimensional bond stress-slip curves (a) RAC, (b) HFRAC

According to the different trends of the dimensionless bond stress-slip curves, the relationship between τ/τ_u and s/s_u was established through experimental data.

The bond stress-slip relationship of HH20, HH100, HH200, HH300, HN20 and HN100 was shown in Eq. (4), and the fitting curve is shown in Fig. 13. The relationship is suitable for HFRAC after being exposed to temperature from 20°C to 300°C and RAC from 20°C to 100°C.

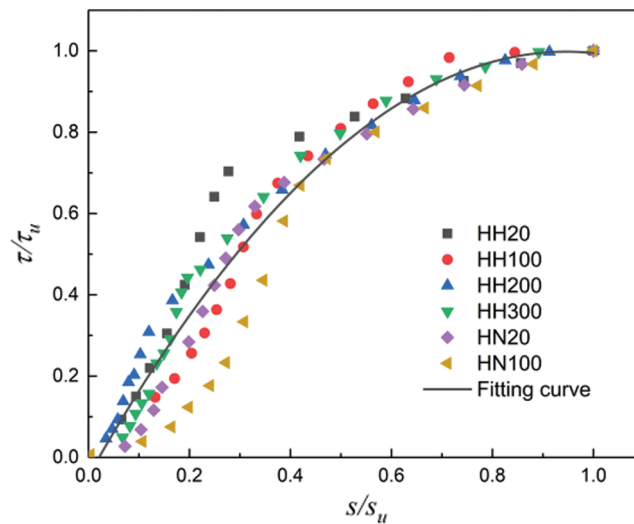


Figure 13: Convex dimensionless bond stress-slip fitting curve

$$\frac{\tau}{\tau_u} = -0.046 + 2.21 \left(\frac{s}{s_u} \right) - 1.17 \left(\frac{s}{s_u} \right)^2 \quad R^2 = 0.914 \quad (4)$$

The bond stress-slip relationship of HH400, HN200, HN300 and HN400 was shown in Eq. (5), and the fitting curve was shown in Fig. 14. The relationship was suitable for HFRAC after being exposed to temperature from 300°C to 400°C and RAC from 100°C to 400°C.

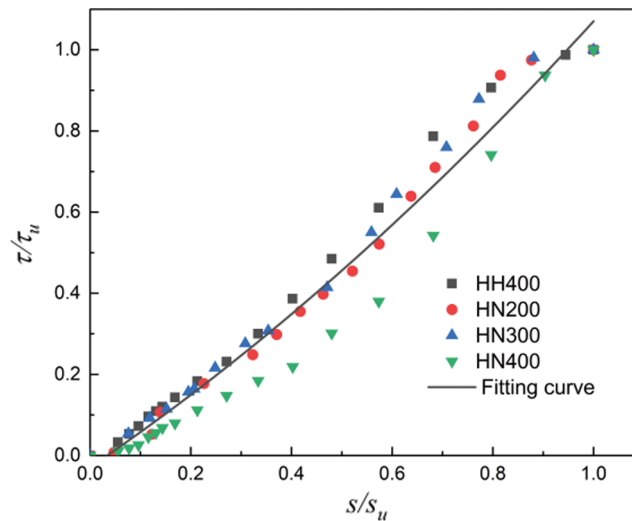


Figure 14: Concave dimensionless bond stress-slip fitting curve

$$\frac{\tau}{\tau_u} = -0.029 + 0.84 \left(\frac{s}{s_u} \right) + 0.26 \left(\frac{s}{s_u} \right)^2 \quad R^2 = 0.903 \quad (5)$$

The area under the bond stress-slip curve (AUC) can reflect the energy consumption during the pull-out test of BFRP bars, and higher the value, the more energy consumption. The AUC value of each group of specimens was calculated by Graphpad Prism software, as shown in Fig. 15. The AUC of the HFRAC specimens increased first with the increase of temperature, reaching a peak at 200°C, an increase of 4.6%; then rapidly decreased after 200°C, only 60.9% and 24.4% at 300°C and 400°C, respectively. As a whole, the AUC of RAC specimens gradually decreased with the increase of temperature. At 200°C, the AUC of RAC specimens decreased by 26.8%. Similar to HFRAC specimens, it decreased significantly after 200°C, and only 41.3% and 21.2% at 300°C and 400°C, respectively. This was related to the high-temperature carbonization of the epoxy resin and the failure of the surface ribs. Besides, with the increase of temperature, the AUC value difference between RAC and HFRAC increased gradually before 200°C and then decreased gradually after 200°C. The AUC of RAC and HFRAC specimens was basically the same at 400°C. The above results also reflected that the key factor controlling the bond properties changed from concrete performance to the BFRP bar performance with the increase of temperature.

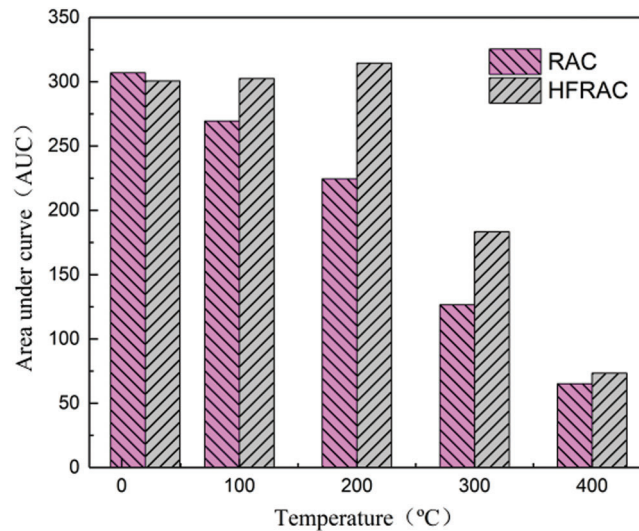


Figure 15: Area enclosed by bond stress-slip curve and abscissa after different exposure temperatures

5 Conclusion

The bond behavior (failure modes, bond strength, bond stress-slip curves) between BFRP bars and hybrid fiber recycled aggregate concrete (HFRAC) after being exposed to different temperatures was investigated. The effects of temperature, hybrid fiber, properties of concrete and BFRP bars on the bond stress-slip relationship between RAC and BFRP bars were discussed. Based on the test results, the following conclusions can be drawn:

1. After the same temperature treatment, the bond properties between HFRAC were better than that of RAC. The slope of bond stress-slip curve decreased with the increase of temperature, which indicated that the bond elastic modulus decreased with the increasing exposure temperature.
2. When the exposure temperature was lower than 300°C, the bond strength was determined by the concrete strength. However, when the exposure temperature was higher than 300°C, the bond strength was controlled by the strength of BFRP bars due to the significant degradation of the properties of BFRP bars.
3. The bond stress-slip curve changed from convex to concave with the increase of exposure temperature. However, the transition temperatures of RAC and HFRAC were 100°C and 300°C, respectively. This indicated that the damage of high temperature to the bond performance between RAC and BFRP bars could be reduced by the incorporation of hybrid fibers.
4. The values of area under bond stress-slip curves (AUC) were calculated to evaluate the energy consumption during the pull-out test of BFRP bars. The AUC values of RAC gradually decreased with increasing exposure temperature, which indicated that high temperature increased the brittleness of RAC. The AUC values of HFRAC were higher than that of RAC, indicating that the incorporation of hybrid fibers improved the toughness of RAC.
5. The relationship between τ/τ_u and s/s_u in the dimensionless bond stress-slip ascending section was established, which was in good agreement with the test results. This can be used as an experimental and theoretical reference for fire prevention design and fire safety evaluation of FRP bar reinforced fiber recycled concrete structures.

Funding Statement: General Program of National Natural Science Foundation of China (Grant No. 51479168) and The Natural Science Foundation Project of Liaoning Provincial Department of Education, China (Grant No. JYL201915404).

Conflicts of Interest: The authors declare that they have no conflicts of interest to report regarding the present study.

References

1. Xiao, J. Z., Li, W. G., Fan, Y. H., Huang, X. (2012). An overview of study on recycled aggregate concrete in China (1996–2011). *Construction and Building Materials*, 31, 364–383. DOI 10.1016/j.conbuildmat.2011.12.074.
2. Mcneil, K., Kang, T. H. (2013). Recycled concrete aggregates: A review. *International Journal of Concrete Structures and Materials*, 7(1), 61–69. DOI 10.1007/s40069-013-0032-5.
3. Yehia, S., Helal, K., Abusharkh, A., Zaher, A., Istaitiyeh, H. (2015). Strength and durability evaluation of recycled aggregate concrete. *International Journal of Concrete Structures and Materials*, 9(2), 219–239. DOI 10.1007/s40069-015-0100-0.
4. Yang, H. F., Qin, Y. H., Liao, Y., Chen, W. (2016). Shear behavior of recycled aggregate concrete after exposure to high temperatures. *Construction and Building Materials*, 106, 374–381. DOI 10.1016/j.conbuildmat.2015.12.103.
5. Choi, H. B., Yi, C. K., Cho, H. H., Kang, K. I. (2010). Experimental study on the shear strength of recycled aggregate concrete beams. *Magazine of Concrete Research*, 62(2), 103–114. DOI 10.1680/mac.2008.62.2.103.
6. Sheen, Y. N., Wang, H. Y., Juang, Y. P., Le, D. H. (2013). Assessment on the engineering properties of ready-mixed concrete using recycled aggregates. *Construction and Building Materials*, 45, 298–305. DOI 10.1016/j.conbuildmat.2013.03.072.
7. Thomas, C., Setien, J., Polanco, J. A., Alaejos, P., De Juan, M. S. (2013). Durability of recycled aggregate concrete. *Construction and Building Materials*, 40, 1054–1065. DOI 10.1016/j.conbuildmat.2012.11.106.
8. Tahmouresi, B., Koushkbaghi, M., Monazami, M., Abbasi, M. T., Nemati, P. (2019). Experimental and statistical analysis of hybrid-fiber-reinforced recycled aggregate concrete. *Computers and Concrete*, 24(3), 193–206.
9. Banthia, N., Majdzadeh, F., Wu, J., Bindiganavile, V. (2014). Fiber synergy in hybrid fiber reinforced concrete (HyFRC) in flexure and direct shear. *Cement & Concrete Composites*, 48(48), 91–97. DOI 10.1016/j.cemconcomp.2013.10.018.
10. Won, J., Park, K., Park, C. (2008). Performance of hybrid fiber reinforced concrete at elevated high temperature. *Journal of the Korea Concrete Institute*, 20(3), 325–333. DOI 10.4334/JKCI.2008.20.3.325.
11. Yildirim, S. T., Ekinici, C. E., Findik, F. (2010). Properties of hybrid fiber reinforced concrete under repeated impact loads. *Russian Journal of Nondestructive Testing*, 46(7), 538–546. DOI 10.1134/S1061830910070090.
12. Purdue ECT Team (2007). FRP Rebar (AFRP, CFRP, GFRP). ECT Fact Sheets.
13. Wang, Z., Zhao, X. L., Xian, G. J., Wu, G., Raman, R. K. et al. (2017). Long-term durability of basalt- and glass-fibre reinforced polymer (BFRP/GFRP) bars in seawater and sea sand concrete environment. *Construction and Building Materials*, 139, 467–489.
14. Choo, J. F., Choi, Y. C., Kwon, S. J., Park, K. T., Yoo, S. W. (2018). Low-cycle flexural fatigue behavior of concrete beam reinforced with hybrid FRP-steel rebar. *Advances in Civil Engineering*, 2018(10), 1–13. DOI 10.1155/2018/6986047.
15. Khanfour, M., Refai, A. E. (2017). Effect of freeze-thaw cycles on concrete reinforced with basalt-fiber reinforced polymers (BFRP) bars. *Construction and Building Materials*, 145, 135–146.
16. Dong, Z. Q., Wu, G., Xu, B., Wang, X., Taerwe, L. (2016). Bond durability of BFRP bars embedded in concrete under seawater conditions and the long-term bond strength prediction. *Materials & Design*, 92, 552–562.
17. Dong, Z. Q., Wu, G., Xu, B., Wang, X., Taerwe, L. (2018). Bond performance of alkaline solution pre-exposed FRP bars with concrete. *Magazine of Concrete Research*, 70(17), 894–904. DOI 10.1680/jmacr.17.00027.
18. Tighiouart, B., Benmokrane, B., Mukhopadhyaya, P. (1999). Bond strength of glass FRP rebar splices in beams under static loading. *Construction & Building Materials*, 13(7), 383–392. DOI 10.1016/S0950-0618(99)00037-9.

19. Zheng, X. H., Huang, P. Y., Chen, G. M., Tan, X. M. (2015). Fatigue behavior of FRP-concrete bond under hygrothermal environment. *Construction and Building Materials*, 95, 898–909.
20. Bellakehal, H., Zaidi, A., Masmoudi, R., Bouhicha, M. (2014). Behavior of FRP bars-reinforced concrete slabs under temperature and sustained load effects. *Polymers*, 6(3), 873–889. DOI 10.3390/polym6030873.
21. Davalos, J. F., Chen, Y., Ray, I. (2012). Long-term durability prediction models for GFRP bars in concrete environment. *Journal of Composite Materials*, 46(16), 1899–1914. DOI 10.1177/0021998311427777.
22. Nigro, E., Bilotta, A., Cefarelli, G., Manfredi, G., Cosenza, E. (2011). Bond models for FRP bars anchorage in concrete slabs under fire. *Applied Mechanics and Materials*, 82, 533–538.
23. Li, C. C., Gao, D. Y., Wang, Y. L., Tang, J. Y. (2017). Effect of high temperature on the bond performance between basalt fibre reinforced polymer (BFRP) bars and concrete. *Construction and Building Materials*, 141, 44–51.
24. Katz, A., Berman, N., Bank, L. C. (1999). Effect of high temperature on bond strength of FRP rebars. *Journal of Composites for Construction*, 3(2), 73–81. DOI 10.1061/(ASCE)1090-0268(1999)3:2(73).
25. Wang, Z. Q., Ju, Z., Han, Y. L., Li, X. J. (2010). Theoretical analysis on the bond-slip constitutive relationship between FRP bars and concrete under high temperature. *Advanced Materials Research*, 141, 340–343.
26. Kashwani, G. A., Altamimi, A. K. (2014). Evaluation of FRP bars performance under high temperature. *Physics Procedia*, 55, 296–300.
27. ACI Committee 440, ACI 440.3R-12 (2012). *Guide test methods for fiber-reinforced polymers (FRP) for reinforcing or strengthening concrete structures*. American Concrete Institute.
28. Tang, L., Zhang, C., Li, B., Zhang, W. (2017). Experimental study on mechanical properties of BFRP bars under high temperature. *Building Science*, 33(1), 36–40.
29. GB/T50152-2012 (2012). *Standard for test methods of concrete structures*. Beijing, China: China Academy of Building Research.
30. Ergun, A., Kurklu, G., Baspinar, M. S. (2016). The effects of material properties on bond strength between reinforcing bar and concrete exposed to high temperature. *Construction and Building Materials*, 112, 691–698.
31. Zhou, Z., Huo, J., Li, Z. (2019). Test and analysis of bond performance between reinforcement and concrete under high temperature. *Building Structure*, 49(10), 76–80.
32. GB/T 50081-2019 (2019). *Standard for test methods of concrete physical and mechanical properties*. Beijing, China.
33. Xue, W. P., Liu, X. Y., Yao, Z. S., Cheng, H., Li, H. P. (2020). Influence of different damage sources on pore structure of basalt fiber reinforced concrete. *ACTA Composite Materials*, 2, 1–8.
34. Zheng, W. Z., Li, H. Y., Wang, Y. (2012). Compressive behaviour of hybrid fiber-reinforced reactive powder concrete after high temperature. *Materials & Design*, 41, 403–409.
35. Robert, M., Benmokrane, B. (2010). Behavior of GFRP reinforcing bars subjected to extreme temperatures. *Journal of Composites for Construction*, 14(4), 353–360. DOI 10.1061/(ASCE)CC.1943-5614.0000092.
36. Wu, J. Y. (2011). *Study on high temperature performance of basalt fiber composite bars*. China: Institute of Engineering Mechanics, China Earthquake Administration.